Search for gravitational waves from black hole hyperbolic encounters in LIGO-Virgo

Gonzalo Morrás, Juan García-Bellido and Savvas Nesseris

Instituto de Física Teórica UAM/CSIC, Universidad Autónoma de Madrid, Cantoblanco
28049 Madrid, Spain

Phys. Dark Univ. 35 (2022), 100932 [arXiv:2110.08000].

Motivation

- Some models predict dense black hole clusters in our universe
    - Primordial black hole models
    - Models for the centers of galaxies and globular clusters
- Black holes in dense clusters will scatter off each other in hyperbolic orbits.
- Sufficiently close scatters will emit gravitational waves (GWs) detectable by current interferometers on Earth.
- Before this work, no targeted search for close hyperbolic encounters (CHEs) had been carried in GW detectors.

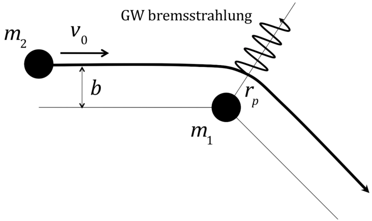

Figure 1: Schematic representation of a Hyperbolic Encounter.

Steps to search for CHE in GW detectors

- Theoretical templates of the GWs emitted by CHE.
- Characterize the signal GWs from CHE leave in laser interferometers.
- Data processing to make the CHE signal stand out over detector noise.
- Develop a trigger to select the data that might contain a CHE. Our trigger will consist on:
  1. Data preselection based on correlations between interferometers.
  2. Convolutional Neural Network to determine which correlations can come from CHE.

CHE templates

- Problem: Scattering of two gravitationally interacting masses m_1 and m_2 with spins $\vec{\mathcal{S}}_1$ and $\vec{\mathcal{S}}_2$.
- No analytical solution in General Relativity (GR).
- Numerical Relativity is computationally cost prohibitive.
- We can use the Post Newtonian (PN) approximation because:
  - BHs do not get as close as in CBC (there is no merger).
  - Accurately following the phase for many cycles is not as critical.
- We take up to leading order spin effects $\rightarrow O(1/c^3) \rightarrow$ 1.5PN.

GW polarizations

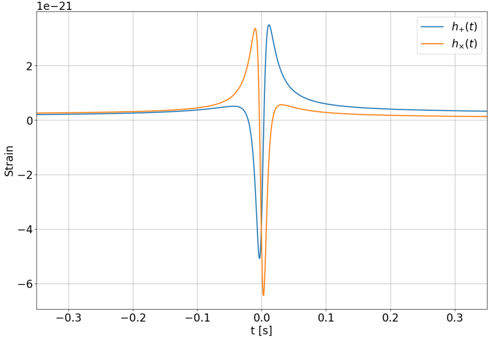

Figure 2: Representative gravitational waves polarization emitted by maximally spinning black holes with $m_1 = 20M_\odot$, $m_2 = 15M_\odot$, $b = 70GM/c^2$, $e_{t0} = 1.1$, $\Phi_0 = 0$, $\theta_1^i = 0.5$ rad, $\phi_1^i = 0.35$ rad, $\theta_2^i = 0.8$ rad, $\phi_2^i = 1$ rad. $t = 0$ represents the time of closest approach.

- Quadrupolar nature of the GWs $\rightarrow f_{\mathrm{GW}} = 2f_{\mathrm{orbit}}$.
- CHE perform "half" of an orbit $\rightarrow$ GWs from CHE perform one oscillation.

Projected GWs into the detector

- The signal the GWs leave in the interferometers is simulated by projecting them into each detector and taking into account light travel time delays.

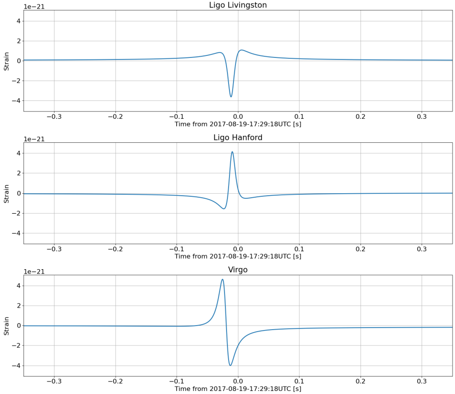

Figure 3: Result of projecting the GWs of Fig. 2 into the GW detectors, assuming that they come from $\delta = 1.0$rad, $\alpha = 3.7$rad, with $\psi = 0.2$rad and with the periastron time taking place at 17:29:18 UTC of 2017-08-19 at the center of the Earth.

Data Processing

- Filtering:
  - Below 20Hz $\rightarrow$ large increase in seismic and thermal noise.
  - Above 800Hz $\rightarrow$ small amount of CHE signal.
  - Remove noise dominated frequencies applying 20-800Hz band-pass.
- Whitening
  - Whiten to weigh down the strain in the noisiest regions and make all frequencies have same noise.
- Q transform:
  - GWs from CHEs only perform only one oscillation $\rightarrow$ extended time-frequency structure.

Data processing example

- Inject example CHE in the detector output: $s(t) = s_{exp}(t) + h_{CHE}(t)$
- Filter, whiten and Q transform the data containing the injection.

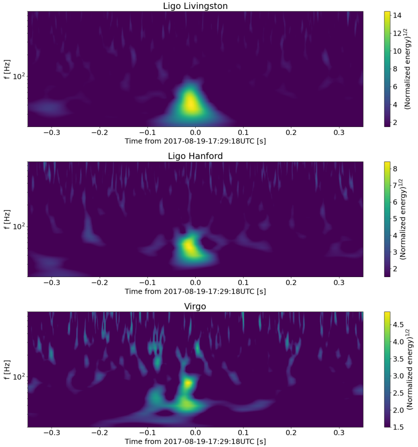

Figure 4: Square root of the normalized energy obtained by applying the data processing to the example CHE injected in the detector data.

Search for CHEs in LIGO-Virgo data

- CHEs look very similar to common blip glitches.
- Coincidences are very important to reject these glitches.
- More detectors online improve search sensitivity.
- Analyze public LIGO-Virgo O2 data with all three detectors in nominal operation $\rightarrow$ 15.3 effective days.
- Since CHEs only do one oscillation burst methods are competitive with and can outperform match filtering techniques for the search.
- Use a two step trigger to look for CHEs:
  1. Correlation trigger.
  2. Neural Network.

Correlation trigger

- We want a loose trigger to preselect events for the Neural Network.
- Look for correlations in the time-frequency domain with Pearson's coeficient:

$$r[x,y] = \frac{\mathrm{cov}(x,y)}{\sigma_x \sigma_y} = \frac{\sum_{n=0}^{N-1}(x_n - \overline{x})(y_n - \overline{y})}{\sqrt{\sum_{n=0}^{N-1}(x_n - \overline{x})^2}\sqrt{\sum_{n=0}^{N-1}(y_n - \overline{y})^2}} ,$$

- Trigger discriminant: $D = a r_{L1-H1} + (1-a) r_{L1-V1}$
- In O2 we determine that for CHE signals, optimally $a \sim 0.67$
- Preselect images with $D > 0.3$

Testing correlation trigger with injections

- What fraction of CHEs can we detect as a function of their SNR?
- We inject CHEs with random parameters and run the correlation trigger over them.

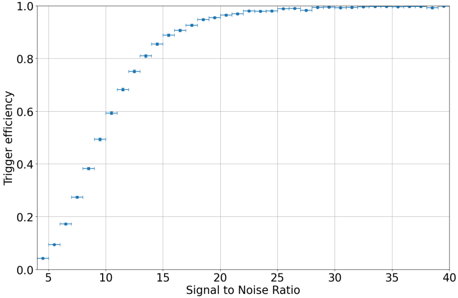

Figure 5: Trigger efficiency as a function of the signal to noise ratio of the injected events.

- We are accepting most events with SNR > 10.

Trigger False Alarm Rate

- We estimate the number of expected noise events by running the trigger on shifted data.
- As expected, events with larger discriminant are increasingly uncommon.

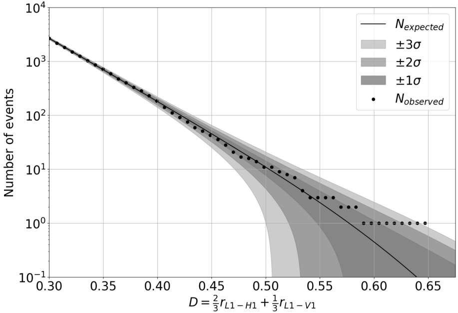

Figure 6: Number of events above a certain discriminant observed and expected. $\sigma = \sqrt{N_{expected}}$.

- Total preselected ($D > 0.3$) events in the data: 2704

Neural Network

- We want to classify which of the 2704 preselected images come from noise and which from CHE.
- Neural networks (NN) are mathematical models to analyze data using Machine Learning.

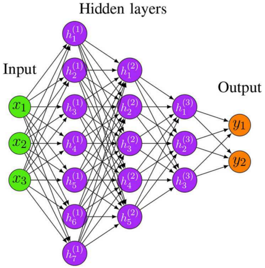

Figure 7: NN sketch. [F. Emmert-Streib (2020)]

- NN input: pixels of the image to be classified.
- NN output: probability of the image to be a CHE.
- Hidden layers:
    - Used for internal calculations only.
    - Contain free parameters to fit training data.

- We use one of the most refined architectures for image classification: Residual Convolutional Neural Network

Image samples

- Put the normalized energy of the three detectors in the same image.
- Image duration: 0.7s

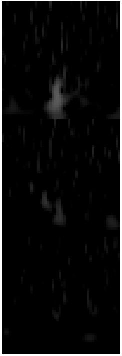

(a) CHE image.

(b) Noise image.

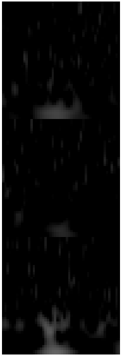

(c) Data Image.

Figure 8: Examples of images used to train and validate our neural network as well as to make predictions on the data.

Neural Network training and performance

- Training the NN means finding the internal parameters such that:
  - If input is a CHE image $\rightarrow$ return 1
  - If input is a noise image $\rightarrow$ return 0
- NN output is then interpreted as CHE probability.
- Train the NN on 64028 noise images and 45356 CHE images.
- We consider an image a CHE candidate if $p_{\text{CHE}} > 0.9$

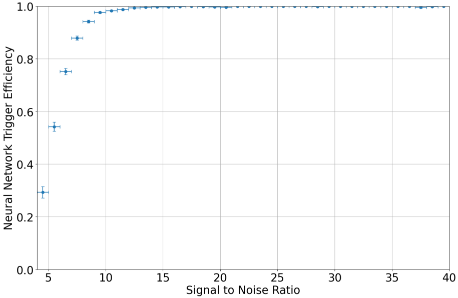

Figure 9: NN trigger efficiency as a function of the signal to noise ratio of the CHE test events.

- We are able to detect most CHEs with signal to noise ratio above 5

Neural Network results on Data

- Distribution of data with CHE probability can be compared with expectation if only noise was present.

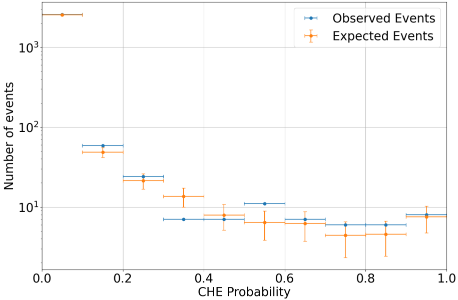

Figure 10: Number of observed events and expected noise events as a function of CHE probability given by the NN. The number of expected noise events is the number of events we would expect to see if the data only contained noise. $\Delta N_{\text{expected}} = \sqrt{N_{\text{expected}}}$

- Consistently more events than expected at high CHE probability.
- At $p_{\text{CHE}} > 0.9 \rightarrow$ We expect 7.5 ± 2.7 noise events and we observe 8.

Most significant events

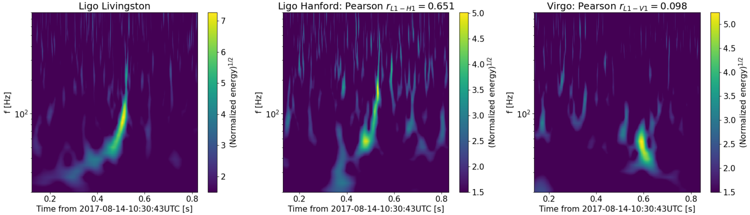

Figure 11: Event with $p_{\text{CHE}} = 0.997$ and correlation discriminant $D = 0.469$. This event is GW170814, the coalescence of two black holes of masses $31M_\odot$ and $25M_\odot$.

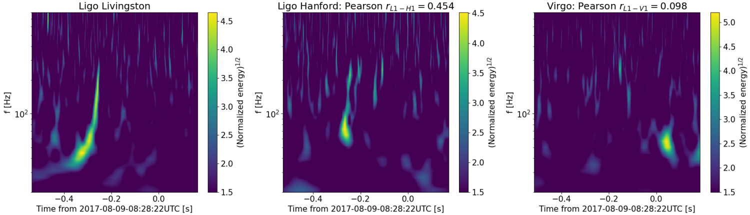

Figure 12: Event with $p_{\text{CHE}} = 0.991$ and correlation discriminant $D = 0.337$. This event is GW170809, the coalescence of two black holes of masses $35M_\odot$ and $24M_\odot$.

Possible CHEs

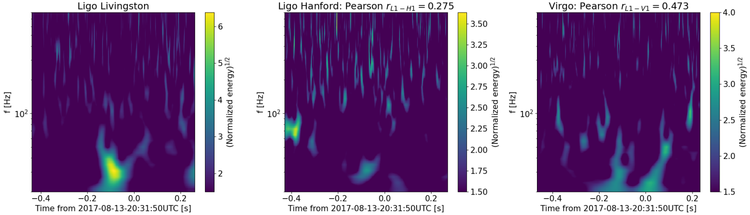

Figure 13: Event with $p_{\text{CHE}} = 0.980$ and correlation discriminant $D = 0.341$.

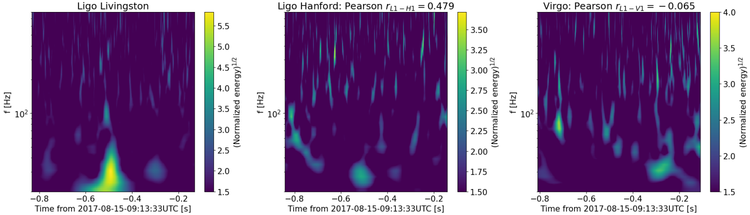

Figure 14: Event with $p_{\text{CHE}} = 0.976$ and correlation discriminant $D = 0.321$.

Conclusions

- Determined GWs emitted by CHEs and characterized how they look in real GW detectors.
- Looked for CHEs in LIGO-Virgo data using burst methods and machine learning.
- Found 2 of the 3 binary black hole mergers contained in the data analyzed.
- Obtained 6 candidate CHEs on which to perform further analysis.
- The number of events is consistent with just noise.

Backup Slides

Backup Slides

Hamiltonian Formulation of the problem

- Hamiltonian of the system:

$$H(\vec{r},\vec{p},\vec{S}_1,\vec{S}_2) = H_{\rm N}(\vec{r},\vec{p}) + H_{\rm 1PN}(\vec{r},\vec{p}) + H_{\rm SO}(\vec{r},\vec{p},\vec{S}_1,\vec{S}_2) + O\left(\frac{1}{c^4}\right) ,$$

where

$$H_{\rm N}(\vec{r},\vec{p}) = \frac{p^2}{2} - \frac{1}{r} ,$$

$$H_{\rm 1PN}(\vec{r},\vec{p}) = \frac{1}{c^2}\left(\frac{1}{8}(3\eta-1)(p^2)^2 - \frac{1}{2}\left[(3+\eta)p^2 + \eta(\hat{n}\cdot\vec{p})^2\right]\frac{1}{r} + \frac{1}{2r^2}\right) ,$$

$$H_{\rm SO}(\vec{r},\vec{p},\vec{S}_1,\vec{S}_2) = \frac{1}{c^2 r^3}(\vec{r}\times\vec{p})\cdot\vec{S}_{\rm eff} ,$$

- To get the equations of motion we use Poisson's brackets:

$$\{r_i, p_j\} = \delta_{ij} ,$$
$$\{S_{1i}, S_{1j}\} = \epsilon_{ijk} S_{1k} ,$$
$$\{S_{2i}, S_{2j}\} = \epsilon_{ijk} S_{2k} .$$

Solution for the orbit

- After some manipulation, the equations of motion can be efficiently solved to obtain the orbit.
- The orbit will depend on:
  - Black hole masses m_1, m_2
  - Black hole initial spins $\vec{S}_1$, $\vec{S}_2$
  - Initial eccentricity e_{t0}
  - Impact parameter b
  - Initial orbital azimutal angle Φ_0
  - Orbital inclination angle Θ

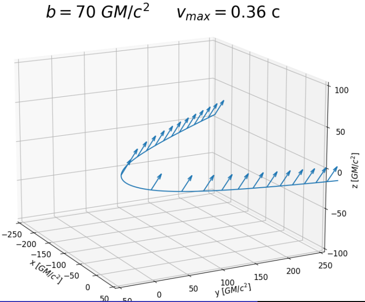

Figure 15: Example of an orbit for maximally spinning black holes with $m_1 = 20M_\odot$, $m_2 = 15M_\odot$, $b = 70Gm/c^2$, $e_{t0} = 1.1$, $\Phi_0 = 0$, $\theta_1^i = 0.5$ rad, $\phi_1^i = 0.35$ rad, $\theta_2^i = 0.8$ rad, $\phi_2^i = 1$ rad. The arrow represents $\vec{S}_{\text{eff}}$.

GWs derived from the orbit

- GWs can computed from the orbit.
- Use formula with up to leading order spin effects:

$$
\begin{aligned}
h_\times = {} & 4\frac{Gm\eta}{c^4R'}\Big\{[-(\boldsymbol{p}\cdot\boldsymbol{n})(\boldsymbol{q}\cdot\boldsymbol{n})z+(\boldsymbol{p}\cdot\boldsymbol{v})(\boldsymbol{q}\cdot\boldsymbol{v})]-\frac{\delta}{c}[(\{[3(\boldsymbol{N}\cdot\boldsymbol{n})\dot{r}-(\boldsymbol{N}\cdot\boldsymbol{v})](\boldsymbol{q}\cdot\boldsymbol{n})-3(\boldsymbol{N}\cdot\boldsymbol{n})(\boldsymbol{q}\cdot\boldsymbol{v})\}(\boldsymbol{p}\cdot\boldsymbol{n})-3(\boldsymbol{N}\cdot\boldsymbol{n})(\boldsymbol{q}\cdot\boldsymbol{n})(\boldsymbol{p}\cdot\boldsymbol{v}))z \\
& +2(\boldsymbol{p}\cdot\boldsymbol{v})(\boldsymbol{q}\cdot\boldsymbol{v})(\boldsymbol{N}\cdot\boldsymbol{v})]+\frac{1}{6c^2}[6(1-3\eta)(\boldsymbol{N}\cdot\boldsymbol{v})^2(\boldsymbol{p}\cdot\boldsymbol{v})(\boldsymbol{q}\cdot\boldsymbol{v})+([(6\eta-2)(\boldsymbol{N}\cdot\boldsymbol{v})^2(\boldsymbol{q}\cdot\boldsymbol{n})+(48\eta-16)(\boldsymbol{N}\cdot\boldsymbol{v})(\boldsymbol{N}\cdot\boldsymbol{n})(\boldsymbol{q}\cdot\boldsymbol{v})] \\
& \times(\boldsymbol{p}\cdot\boldsymbol{n})+(48\eta-16)(\boldsymbol{N}\cdot\boldsymbol{v})(\boldsymbol{N}\cdot\boldsymbol{n})(\boldsymbol{p}\cdot\boldsymbol{v})(\boldsymbol{q}\cdot\boldsymbol{n})+((-14+42\eta)(\boldsymbol{N}\cdot\boldsymbol{n})^2-4+6\eta)(\boldsymbol{q}\cdot\boldsymbol{v})(\boldsymbol{p}\cdot\boldsymbol{v}))z+(-9\eta+3)(\boldsymbol{q}\cdot\boldsymbol{v}) \\
& \times(\boldsymbol{p}\cdot\boldsymbol{v})v^2+(29+(7-21\eta)(\boldsymbol{N}\cdot\boldsymbol{n})^2)(\boldsymbol{q}\cdot\boldsymbol{n})(\boldsymbol{p}\cdot\boldsymbol{n})z^2+((-9\eta+3)(\boldsymbol{N}\cdot\boldsymbol{n})^2-10-3\eta)(\boldsymbol{q}\cdot\boldsymbol{n})(\boldsymbol{p}\cdot\boldsymbol{n})zv^2+([(-36\eta+12) \\
& \times(\boldsymbol{N}\cdot\boldsymbol{v})(\boldsymbol{N}\cdot\boldsymbol{n})(\boldsymbol{q}\cdot\boldsymbol{n})+((15-45\eta)(\boldsymbol{N}\cdot\boldsymbol{n})^2+10+6\eta)(\boldsymbol{q}\cdot\boldsymbol{v})](\boldsymbol{p}\cdot\boldsymbol{n})+[(15-45\eta)(\boldsymbol{N}\cdot\boldsymbol{n})^2+10+6\eta](\boldsymbol{p}\cdot\boldsymbol{v})(\boldsymbol{q}\cdot\boldsymbol{n}))\dot{r}z \\
& +((45\eta-15)(\boldsymbol{N}\cdot\boldsymbol{n})^2-9\eta+3)(\boldsymbol{q}\cdot\boldsymbol{n})(\boldsymbol{p}\cdot\boldsymbol{n})\dot{r}^2z]+\frac{z^2(\boldsymbol{q}\cdot\boldsymbol{n})}{c^2}[X_2\chi_2(\boldsymbol{p}\cdot(s_2\times N))-X_1\chi_1(\boldsymbol{p}\cdot(s_1\times N))]\Big\}, \\
h_+ = {} & 2\frac{Gm\eta}{c^4R'}\Big\{[((\boldsymbol{q}\cdot\boldsymbol{n})^2-(\boldsymbol{p}\cdot\boldsymbol{n})^2)z+(\boldsymbol{p}\cdot\boldsymbol{v})^2-(\boldsymbol{q}\cdot\boldsymbol{v})^2]-\frac{\delta}{2c}[((\boldsymbol{N}\cdot\boldsymbol{n})\dot{r}-(\boldsymbol{N}\cdot\boldsymbol{v}))z(\boldsymbol{p}\cdot\boldsymbol{n})^2-6z(\boldsymbol{N}\cdot\boldsymbol{n})(\boldsymbol{p}\cdot\boldsymbol{n})(\boldsymbol{p}\cdot\boldsymbol{v})+(-3(\boldsymbol{N}\cdot\boldsymbol{n})\dot{r} \\
& +(\boldsymbol{N}\cdot\boldsymbol{v}))z(\boldsymbol{q}\cdot\boldsymbol{n})^2+6z(\boldsymbol{N}\cdot\boldsymbol{n})(\boldsymbol{q}\cdot\boldsymbol{n})(\boldsymbol{q}\cdot\boldsymbol{v})+2((\boldsymbol{p}\cdot\boldsymbol{v})^2-(\boldsymbol{q}\cdot\boldsymbol{v})^2)(\boldsymbol{N}\cdot\boldsymbol{v})]+\frac{1}{6c^2}[6(\boldsymbol{N}\cdot\boldsymbol{v})^2((\boldsymbol{p}\cdot\boldsymbol{v})^2-(\boldsymbol{q}\cdot\boldsymbol{v})^2)(1-3\eta) \\
& +([6\eta-2](\boldsymbol{N}\cdot\boldsymbol{v})^2(\boldsymbol{p}\cdot\boldsymbol{n})^2+(96\eta-32)(\boldsymbol{N}\cdot\boldsymbol{v})(\boldsymbol{N}\cdot\boldsymbol{n})(\boldsymbol{p}\cdot\boldsymbol{v})(\boldsymbol{p}\cdot\boldsymbol{n})+(-6\eta+2)(\boldsymbol{N}\cdot\boldsymbol{v})^2(\boldsymbol{q}\cdot\boldsymbol{n})^2+(-96\eta+32)(\boldsymbol{N}\cdot\boldsymbol{v}) \\
& \times(\boldsymbol{N}\cdot\boldsymbol{n})(\boldsymbol{q}\cdot\boldsymbol{v})(\boldsymbol{q}\cdot\boldsymbol{n})+[(-14+42\eta)(\boldsymbol{N}\cdot\boldsymbol{n})^2-4+6\eta](\boldsymbol{p}\cdot\boldsymbol{v})^2+[(-42\eta+14)(\boldsymbol{N}\cdot\boldsymbol{n})^2+4-6\eta](\boldsymbol{q}\cdot\boldsymbol{v})^2)z \\
& +((-9\eta+3)(\boldsymbol{p}\cdot\boldsymbol{v})^2+(-3+9\eta)(\boldsymbol{q}\cdot\boldsymbol{v})^2)v^2+([29+(7-21\eta)(\boldsymbol{N}\cdot\boldsymbol{n})^2](\boldsymbol{p}\cdot\boldsymbol{n})^2+[-29+(21\eta-7)(\boldsymbol{N}\cdot\boldsymbol{n})^2](\boldsymbol{q}\cdot\boldsymbol{n})^2)z^2 \\
& +(((-9\eta+3)(\boldsymbol{N}\cdot\boldsymbol{n})^2-10-3\eta)(\boldsymbol{p}\cdot\boldsymbol{n})^2+((-3+9\eta)(\boldsymbol{N}\cdot\boldsymbol{n})^2+10+3\eta)(\boldsymbol{q}\cdot\boldsymbol{n})^2)zv^2+((-36\eta+12)(\boldsymbol{N}\cdot\boldsymbol{v})(\boldsymbol{N}\cdot\boldsymbol{n}) \\
& \times(\boldsymbol{p}\cdot\boldsymbol{n})^2+((-90\eta+30)(\boldsymbol{N}\cdot\boldsymbol{n})^2+20+12\eta)(\boldsymbol{p}\cdot\boldsymbol{v})(\boldsymbol{p}\cdot\boldsymbol{n})+(-12+36\eta)(\boldsymbol{N}\cdot\boldsymbol{v})(\boldsymbol{N}\cdot\boldsymbol{n})(\boldsymbol{q}\cdot\boldsymbol{n})^2+((90\eta-30)(\boldsymbol{N}\cdot\boldsymbol{n})^2 \\
& -12\eta-20)(\boldsymbol{q}\cdot\boldsymbol{v})(\boldsymbol{q}\cdot\boldsymbol{n}))z\dot{r}+([(45\eta-15)(\boldsymbol{N}\cdot\boldsymbol{n})^2-9\eta+3](\boldsymbol{p}\cdot\boldsymbol{n})^2+((15-45\eta)(\boldsymbol{N}\cdot\boldsymbol{n})^2-3+9\eta)(\boldsymbol{q}\cdot\boldsymbol{n})^2)z\dot{r}^2] \\
& +\frac{z^2}{c^2}[(\boldsymbol{p}\cdot\boldsymbol{n})(X_2\chi_2[\boldsymbol{p}\cdot(s_2\times N)]-X_1\chi_1[\boldsymbol{p}\cdot(s_1\times N)])+(\boldsymbol{q}\cdot\boldsymbol{n})(X_1\chi_1[\boldsymbol{q}\cdot(s_1\times N)]-X_2\chi_2[\boldsymbol{q}\cdot(s_2\times N)])\Big\}
\end{aligned}
$$

Antenna Patterns

$$F_{+}(\theta, \phi, \psi) = \frac{1}{2}(1 + \cos^{2}\theta)\cos 2\phi \cos 2\psi - \cos\theta \sin 2\phi \sin 2\psi \,,$$
$$F_{\times}(\theta, \phi, \psi) = \frac{1}{2}(1 + \cos^{2}\theta)\cos 2\phi \sin 2\psi + \cos\theta \sin 2\phi \cos 2\psi \,.$$

- θ and ϕ give the direction of the GW in the frame in which the arms of the interferometer are in the x and y axis.
- ψ measures the polarization of the wave.
- Detectors have different locations and orientations $\rightarrow$ θ, ϕ and ψ are different in each one for a GW coming from a location in the sky with right ascension α and declination δ.
- GWs arrive at different times in different locations due to the light travel time.

Injected signal

- Current detectors are dominated by noise.
- Data processing suppresses the noise, enhancing the signal.

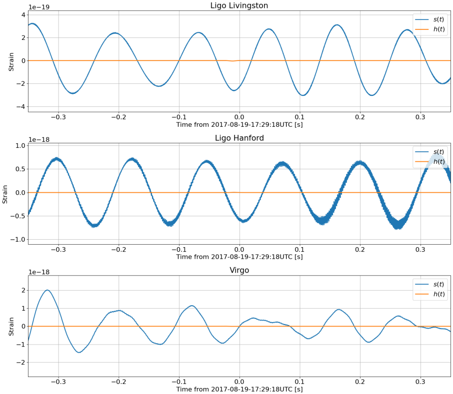

Figure 16: In blue, result $s(t)$ of injecting the example GWs into the experimental strain of the detectors. In orange, the GW signal $h(t)$. The noise is so dominating that the features of the gravitational wave signal can not be seen.

CHE frequency dependance

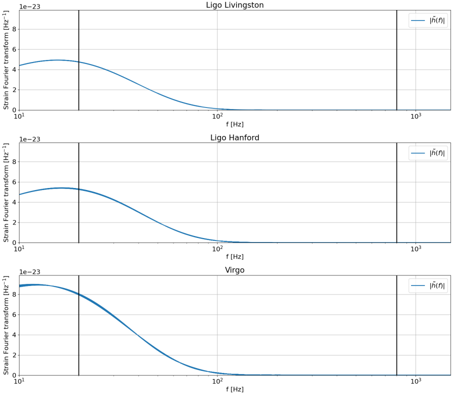

Figure 17: Fourier transform of the gravitational wave shown in Fig. 3. We have marked with black lines the 20-800Hz frequency window we are using to band-pass the strain.

Filtering

- Below 20Hz and above 800Hz data is dominated by noise.
- Remove noise dominated frequencies applying 20-800Hz band-pass.

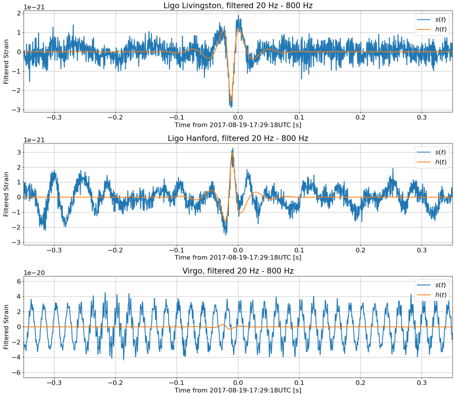

Figure 18: Result of band-pass filtering the example signals within a 20-800Hz window.

Whitening

- The signal in frequencies with more noise is less significant.
- Whiten to make all frequencies have same noise $\tilde{s}_{\text{whiten}}(f) = \frac{\tilde{s}(f)}{\sqrt{S_n(f)}}$.

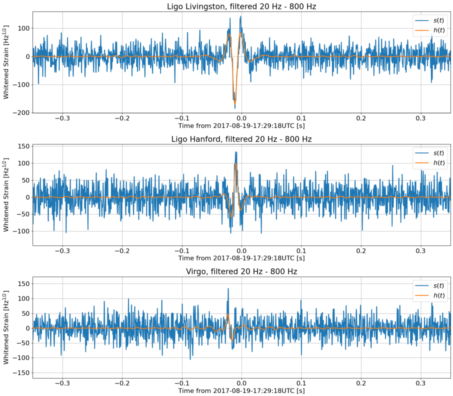

Figure 19: Result of whitening the example filtered signals.

3σ correlated event

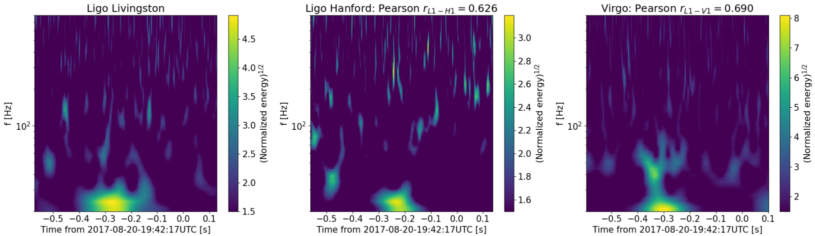

Figure 20: Event with the highest value of the trigger discriminant found in the analyzed data, with a value $D = 0.647$. From our false alarm rate analysis we expect an event like this every 240 days but we got one in 15.3 days of data.

Other CHE candidates I

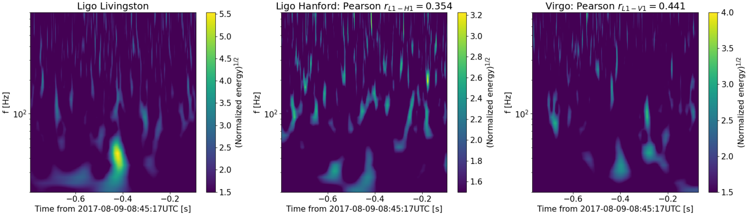

Figure 21: Event with $p_{\mathrm{CHE}} = 0.974$ and correlation discriminant $D = 0.382$.

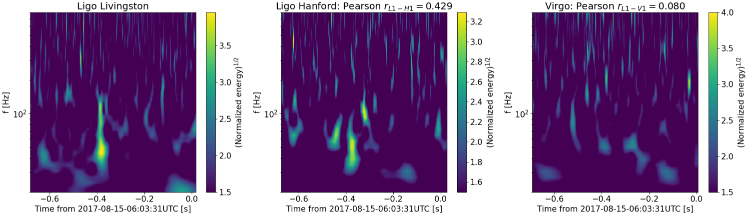

Figure 22: Event with $p_{\mathrm{CHE}} = 0.942$ and correlation discriminant $D = 0.314$.

Other CHE candidates II

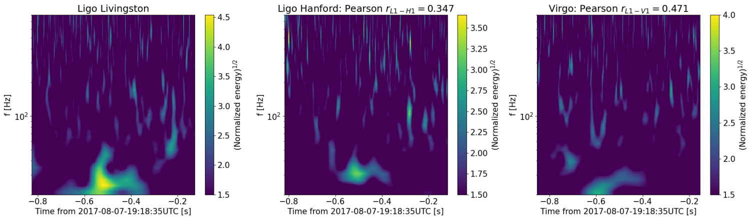

Figure 23: Event with $p_{\text{CHE}} = 0.927$ and correlation discriminant $D = 0.388$..

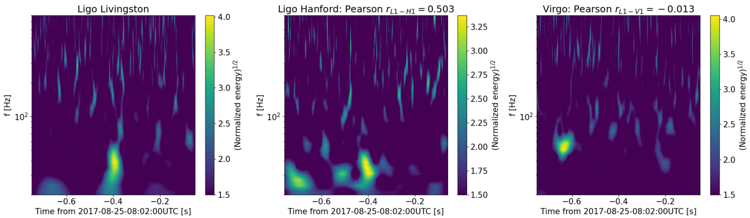

Figure 24: Event with $p_{\text{CHE}} = 0.914$ and correlation discriminant $D = 0.337$.